

Print ISSN

1110-7642

Online ISSN 2735-5039

AIN SHAMS DENTAL JOURNAL

Official Publication of Ain Shams Dental School **June2025 • Vol. 38**

Stem Cells-Derived Exosomes Versus Injectable-Platelet Rich Fibrin effect on Irradiated Submandibular Salivary Glands

Basant Abd El-monaem Mahmoud¹, Marwa M. Abd El-Hameed¹ Nuha Abdul-Fattah Baraka¹

Aim: This study aimed to compare the ameliorative potentials of Injectable-Platelet Rich Fibrin (I-PRF) and Bone marrow mesenchymal stem cells (BM-MSCs) derived exosomes on irradiated rat submandibular salivary glands (SMGs).

Materials and Methods: Forty-nine male albino rats had been divided into 4 main groups (12 rats each) and one rat had been used as doner. Group I served as –ve control while Group II had been exposed to gamma irradiation (single dose of 6 Gy) and the other two groups were injected 24 h post-radiation with a single dose of I-PRF (Group III), exosomes (Group IV). SMG regeneration was assessed in terms of histological changes, ultra-structural changes and TGF- β1 gene expression.

Results: The results showed that compared to the irradiated group all treated groups showed successful regeneration. Our results prove that using I-PRF and Exosomes could be promising in decreasing irradiation side effects on SMG.

Conclusion: BM-MSCs derived exosomes and IPRF had a role in regeneration of irradiated SMG. Our results demonstrated that using IPRF had ameliorative effect in regeneration of irradiated SMG but for a short-term duration unlike exosomes that mediate a better regenerative effect on long term duration.

Keywords: Transmission electron microscope, regeneration, transforming growth factor beta.

 Oral Biology Department, Faculty of Dentistry, Ain Shams University, Cairo, Egypt. Corresponding author: Basant Abd El-monaem Mahmoud, email: basant-abdelmonaem@dent.asu.edu.eg

Introduction

Salivary gland tumors are a histologically varied category of neoplasms in the head and neck area, accounting for 3 to 11% of malignancies in this region. ¹

Salivary glands sustain significant damage during radiation therapy. This results in significant salivary gland hypofunction, leading to numerous problems including xerostomia, dysphagia, oropharyngeal infections. severe dental caries. mucositis.² Regenerative medicine treatment is applied in preclinical studies by using alternative strategies, such as gene therapy, tissue engineering, or cell-based therapy for salivary gland regeneration. Regenerative medicine aims to restore the structure and function of SGs in patients with loss of SGs function due to atrophy. Injectable-Platelet Rich Fibrin (I-PRF) may improve the potential of intrinsic tissue regeneration by stimulating the proliferation and migration of human mesenchymal stem cells (MSCs). ³ I-PRF has been documented to have enhanced anti-inflammatory antimicrobial and properties against several infections, perhaps facilitating expedited tissue regeneration.4 PRF constitutes a three-dimensional fibrin that functions as a matrix scaffold. encapsulating various growth factors. including vascular endothelial growth factor (VEGF), transforming growth factor-beta 1 (TGF-β1), and platelet-derived growth factor (PDGF), which are essential for tissue regeneration. ⁵

Many preclinical and clinical trials using exosomes for tissue regeneration have been conducted. For SGs, Bone marrow mesenchymal stem cells (BM-MSCs) derived exosomes were reported to be a potential candidate for the treatment of salivary hypofunction. ^{6,7,8}

Studies that demonstrated the effect of exosomes directly on irradiated SMGs were deficient. Also, no histopathological studies were conducted on the regenerative potential of I-PRP and BM-MSCs derived exosomes on irradiated submandibular salivary glands. Therefore, the present study was proposed to provide new research stand through exploring the possible therapeutic effect of local injection of IPRF and exosomes on regeneration of irradiated submandibular salivary glands.

Materials and methods Animal model and ethical statement

Forty-nine male albino rats weighing between (150-200 grams) had been housed in the medical research center, Faculty of Medicine, Ain Shams University, under controlled temperature and dark light cycle. They had been fed with standard diet and fresh tap water according to institution guidelines of Ain Shams University Ethical Committee (approval number: FDASU-Rec IM 052331).

Sample size

Sample size calculation was performed using G*Power version 3.1.9.7 based on the results of a previous study. A power analysis was designed to have adequate power to apply a two-sided statistical test to reject the null hypothesis that there is no difference between groups. By adopting an alpha level of (0.05) and a beta of (0.2), i.e. power = 80% and an effect size (d) of (0.65) calculated based on the results of a previous study. The predicted sample size (n) was (48), i.e., 6 samples per sub-group to detect and compare the effect of (BM-MSCs)-derived exosomes versus (IPRF).

Study design

Forty-nine male albino rats had been divided into 4 main groups (12 rats each) and one rat had been used as doner. Group I (-ve control group): This group served as -ve control group and had been injected with (100µl) phosphate buffered saline in the SMG. Group II (+ve control group): This

group had been exposed to gamma irradiation (single dose of 6 Gy)and 24 hours later they had received (100µl) phosphate buffered saline in the SMG. Group III (irradiated group treated by IPRF): This group received a single dose of 6Gy irradiation and after 24 hours they received an intraglandular injection of single dose of IPRF (100 µl)⁹, Group IV (irradiated group treated by BM-MSCs exosomes): This group received a single dose of 6Gy irradiation, and after 24 hours they received an intraglandular injection of a single dose of BM-MSCs derived exosome (50µg) suspended in (100 μl) phosphate buffered saline.⁸ Each group was divided into subgroup A in which the rats were sacrificed after 7 days and subgroup B in which the rats were scarified after 14 days post-radiation.

Irradiation procedure

The rats were irradiated with a single dose of 6 Gy. Whole-body gamma-irradiation was executed at the National Center for Radiation Research and Technology (NCRRT), Atomic Energy Authority, Cairo, Egypt.

BM-MSCs Exosomes preparation

Exosomes were extracted from the supernatants of BM-MSCs grown overnight in Roswell Park Memorial Institute (RPMI) free of Fetal Bovine serum (FBS). To obtain exosomes. cell-free supernatants centrifuged at 10,000 ×g at 4 °C for 20 minutes to eliminate debris. Centrifugation was subsequently conducted at 100,000 ×g (Beckman Coulter Optima L-90K ultracentrifuge) for one hour at 4 °C. Cellfree supernatants were subsequently washed in serum-free media 199 containing 25 mM N-2-Hydroxy Ethyl Piperazine-N'-2-Ethane Sulfonic acid (Sigma-Aldrich®) subjected to a second ultracentrifugation identical circumstances. 10 cytometry had been used for exosomes characterization and these procedures had

been done at Nawah scientific research labs, Almokattam, Cairo, Egypt.

IPRF preparation

For I-PRF preparation, one male albino rat had been anesthetized by ketamine (50 mg/kg) then 3.5 ml blood sample without anticoagulant had been collected from retro orbital plexus with capillary tube and rapidly centrifuged for I-PRF preparation at 700 rpm for 3 min (60×g) at room temperature by Duo centrifuge (process of PRF, Nice, France). The upper liquid layer had been collected as I-PRF. This had been done at Faculty of Medicine Ain Shams Medical Research Institute (MASRI).

Specimen preparation

The animals had been sacrificed by intracardiac overdose of sodium thiopental at days 7 and 14 post-radiation (6 rats at each time for each group) and the submandibular salivary glands had been dissected. Half of the right submandibular glands had been fixed for one hour in buffered glutaraldehyde (2.5%) at 4 temperature for the $^{\mathrm{o}}\mathrm{C}$ transmission electron microscope examination, and the other half of the specimen had been kept at −20 °C in Eppendorf tubes for further analysis of TGFβ1 gene expression. The left submandibular glands had been washed in saline solution and fixed in 10% buffered formalin for 24 hr for histological preparation of H&E-stained sections.9

Histomorphometric analysis

The histopathological changes in submandibular salivary glands were evaluated in terms of the area fraction of acini and fibrosis. Images were first enhanced for contrast and brightness and inspected by the Image J program (Image J,1.41a, NIH, USA) at Oral Pathology Department, Faculty of Dentistry, Ain shams University to determine both the area of acini and fibrosis per field.

These were measured blindly by the observer. For each subgroup, 4 representative photographs of H&E-stained sections at (x200) magnifications were used for analysis.

Glandular ultra-structural examination

Specimens were examined for the presence of pyknotic nuclei, cytoplasmic vacuoles, multiple atypical secretory granule and dilated RER in glandular acini and intercalated ducts. Also, basal striations with cristae of mitochondria of striated ducts had been observed. The architecture of the granular convoluted tubule and its granules were inspected as well. Pseudostratified appearance of excretory ducts and infiltration of inflammatory cells were also examined.

Specimens were inspected and photographed using a transmission electron microscope (TEM) SEOTEM-100 (SUMY Electron Optics – Ukraine) in the Electron Microscopy unit in the Geology Department, Faculty of Sciences, Ain Shams University.

Gene expression detection for TGFβ-1 using qRT-PCR

Total RNA had been isolated using Qiagen RNeasy extraction kit (RNeasy Mini kit, cat no: 74104. Oiagen, Hilden, Germany) according the manufacturer's to instructions. Reverse transcription of total RNA into cDNA had been performed using a specific kit QuantiTect Reverse Transcription Kit, cat. No. 205310, (Qiagen, Hilden, Germany). This kit includes specific primer probes for the studied target gene (TGFβ-1) and reference housekeeping gene (GAPDH). RT-PCR master mix had been prepared by mixing the kit reagents according to the manufacturer's instructions to reach a total volume of 50 µl. PCR amplification had been performed using realtime PCR (QuantiTect primer assay, cat no: [Rn Tgfb1 1 SG 249900 QuantiTect Primer Assay, ID: QT00187796, (Qiagen, Germany) and QuantiTect SYBR Green PCR

Kit cat no: 204141 (Qiagen, Germany) and HS GAPDH 1 SG, ID: OT00079247 OuantiTect Primer Assay cat no: 249900, as housekeeper gene. These procedures were done in Global research labs, medical center 2, Nasr city, Cairo, Egypt.

Statistical methods

The normality of the numerical data was examined by checking the distribution of data and using tests of normality (Kolmogorov-Smirnov and Shapiro-Wilk tests). Data showed a normal (parametric) distribution. Data were presented as mean, standard deviation (SD), median, and range values. Two-way ANOVA test was used for comparisons between the groups as well as the comparison between times. When ANOVA test is significant Bonferroni's posthoc test was used for pair-wise comparisons. Statistical analysis was performed with IBM SPSS Statistics for Windows, Version 23.0. Armonk, NY: IBM Corp. The significance level was set at $P \le 0.05$.

Results

Histopathological examination

SMG of the control group was formed of normal seromucous acini, intercalated ducts (IDs), striated ducts (SDs), excretory ducts (EDs) and granular convoluted tubule (GCTs)(fig.1a,1b,2a,2b). On the other hand, SMG of irradiated subgroup IIA revealed that both serous acini and granular elements showed ill-defined outline with hyperchromatic nuclei and multiple cytoplasmic vacuoles of variable sizes. The nuclei of acinar cells appeared pyknotic and hyperchromatic and acinar cell cytoplasm had many vacuolations of variable sizes (fig. 1c). EDs showed loss of pseudostratified hyperchromatic appearance, nuclei. degenerating lining cells and stagnation of secretion in its lumen. Hyalinization of the surrounding connective tissue septa was

observed (Fig. 2c). After 14 days, Irradiated subgroup IIB sections revealed that serous acini were more shrunken, the nuclei of acinar cells appeared more pyknotic and hyperchromatic and acinar cell cytoplasm had many vacuolations of variable sizes. SDs showed almost degenerated cells with stagnation of secretion, loss of basal striations and hyperchromatic nuclei (fig. 1d). EDs showed reduction in cell height, loss of pseudostratified appearance and stagnation of secretion in its lumen (fig.2d). GCT showed partial loss of outline and hyperchromatic nuclei (fig. 1d).

SMG of subgroup IIIA presented acini with an almost spherical shape consisting of pyramidal cells with basophilic cytoplasm and rounded basally situated nuclei (fig. 1e). The majority of SDs were lined by a single layer of columnar cells with rounded centrally placed nuclei and it showed eosinophilic cytoplasm with basal striations as well. EDs were lined by pseudostratified columnar epithelium with goblet cells with areas of degeneration, cytoplasmic vacuoles, and hyperchromatic nuclei. However some other EDs showed stagnation of secretion in its lumen. Hyalinization and extravasation of RBCs around EDs were also evident in other sections (fig. 2e) . GCTs showed almost regular configurations with basal rounded hyperchromatic nuclei (fig. 1e).

In subgroup IIIB, some of serous acini were similar to subgroup IIIA, however cytoplasmic vacuoles and hyperchromatic nuclei were more in this subgroup. The SDs and ED were like subgroup IIIA but there were some cytoplasmic vacuolations and loss of stratifications in some areas of SDs and some areas of degeneration and cytoplasmic vacoules in cells of EDs (fig. 1f, 2f). GCTs were lined by columnar cells with granular cytoplasm with eosinophilic centrally situated nuclei; however, some other cells were degenerated and others cytoplasmic vacuolations (fig. 2f).

Regarding subgroup IVA and subgroup IVB, the serous acini were almost spherical in shape with basophilic cytoplasm however some were more shrunken in subgroup IVA (fig. 1g). The SDs of subgroup IVA and subgroup IVB were lined by a single layer of columnar cells with rounded centrally placed nuclei, and it showed eosinophilic cytoplasm with basal striations but in subgroup IVA there were some cytoplasmic vacuolations and loss of stratifications in some areas (fig. 2g). ED of subgroup IVA and subgroup IVB were lined by pseudostratified columnar epithelium with goblet cells, however subgroup IVA EDs showed a small area of cytoplasmic vacuoles and stagnation of secretion in its lumen and subgroup IVB EDs were lined by flat cells in some areas with empty lumens in some of them and stagnant secretion in the others (fig. 2g, 2h). EDs were surrounded by congested BVs engorged with RBCs in subgroup IVA (fig. 2g). GCTs of both subgroups IVA and IVB were lined by columnar cells with granular eosinophilic cytoplasm with centrally situated nuclei, however some cells other showed cytoplasmic vacuolations in subgroup IVA (fig. 1g, 1h). Some of GCTs in subgroup IVB may show an ill-defined outline with degenerated cells.

Histomorphometric analysis

The histological changes in submandibular glands were evaluated in terms of the total surface area percentage of acini and fibrosis. The highest mean value of area fraction of fibrosis was recorded in subgroup IIA, followed by subgroup IVA, subgroup IIIA was lower and the lowest value in subgroup IA (fig. 5). ANOVA test revealed a statistically significant difference between groups (P=0.001).

Also, the highest mean value of area fraction of acini was recorded in subgroup IA, followed by subgroup IIIA, then subgroup IVA and the lowest value in

subgroup IIA (fig. 5). ANOVA test revealed a statistically significant difference between subgroups (P=0.008).

Also, with the second duration (14 days), the highest mean value of area fraction of fibrosis was recorded in group IIB, followed by group IIIB, then the group IVB and the lowest value in group IB. Also, there was a highest mean value of area fraction of acini was recorded in group IB, followed by group IVB, then group IIIB and the lowest value in group IIB (fig. 5). ANOVA test revealed a statistically significant difference between groups (P=0.001).

Glandular ultra-structural results

In our study, ultra-structure examination of SMG of control group revealed acini with basally situated rounded nucleus (N) and normal appearance of secretory granules (SG) (fig. 3a). SDs showed deep basal enfolding, between which numerous mitochondria and numerous RER (R) were stacked. Open faced nuclei with peripheral chromatin condensation were observed as well (fig. 4b).

On the other hand, ultrastructural examination of irradiated groups at both durations revealed that there was condensation and clumping of chromatin into masses of the nuclei of the glandular acini. Acinar cells showed multiple cytoplasmic vacuoles and multiple irregular shapes of secretory granules. There was also detachment of cellular junctions between the atrophied acini (fig. 3c).

Cells of IDs appeared cuboidal to flat in some sections with pyknotic nucleus, dilated RER and abnormal mitochondria (fig. 4c). The dilated lumen was also evident. Cells of SDs revealed multiple cytoplasmic vacuoles, pyknotic nuclei, loss of basal striations and some mitochondria with damaged cristae were displaced apically (fig. 4d).

Cells of GCTs revealed variation in size, shape and position of the nuclei

(pleomorphism). Some pyknotic nuclei are also evident. Many electron-dense secretory granules were also found. Cells of EDs showed loss of pseudostratified appearance and nuclei were variant in size and shape. The connective tissue septa appeared with multiple vacuolations, and blood vessels were engorged with RBCs.

The ultrastructure of IPRF group in both durations showed some acini with atypical, atrophied nuclei. numerous secretory granules, and some cytoplasmic vacuoles were also seen (fig. 3f). The associated blood vessel was engorged with RBCs (fig. 3e). The IDs were lined by cuboidal cells with cytoplasmic indented membrane centrally located hyperchromatic nuclei. Cells of SD in subgroup IIIA showed areas of basal striation while other areas showed loss of basal striation, however in subgroup IIIB they appeared normal (fig. 4e). GCTs and EDs revealed normal appearance as well. There was interstitial fibrosis and abnormal fibroblast with large plumb associated with blood vessel engorged with RBCs and surrounded by numerous collagen bundles in subgroup IIIA (Fig. 3e).

subgroup IVA revealed acini with open faced nuclei and prominent nucleolus, however some other pleomorphic nuclei were also seen. Some cells of IDs appeared with large open-faced nuclei while other cells showed pyknotic pleomorphic nuclei (fig. 4g). Moreover, there were cytoplasmic vacuoles. The SDs appeared normal. The connective tissue septa appeared infiltrated with inflammatory cells and BVs appeared engorged with RBCs (fig.3g). Subgroup IVB showed many acini with apparent normal size and shape, IDs and GCTs had normal appearance. The EDs were lined by pseudostratified epithelium with large, rounded nuclei, some of them appeared open faced while others appeared pyknotic.

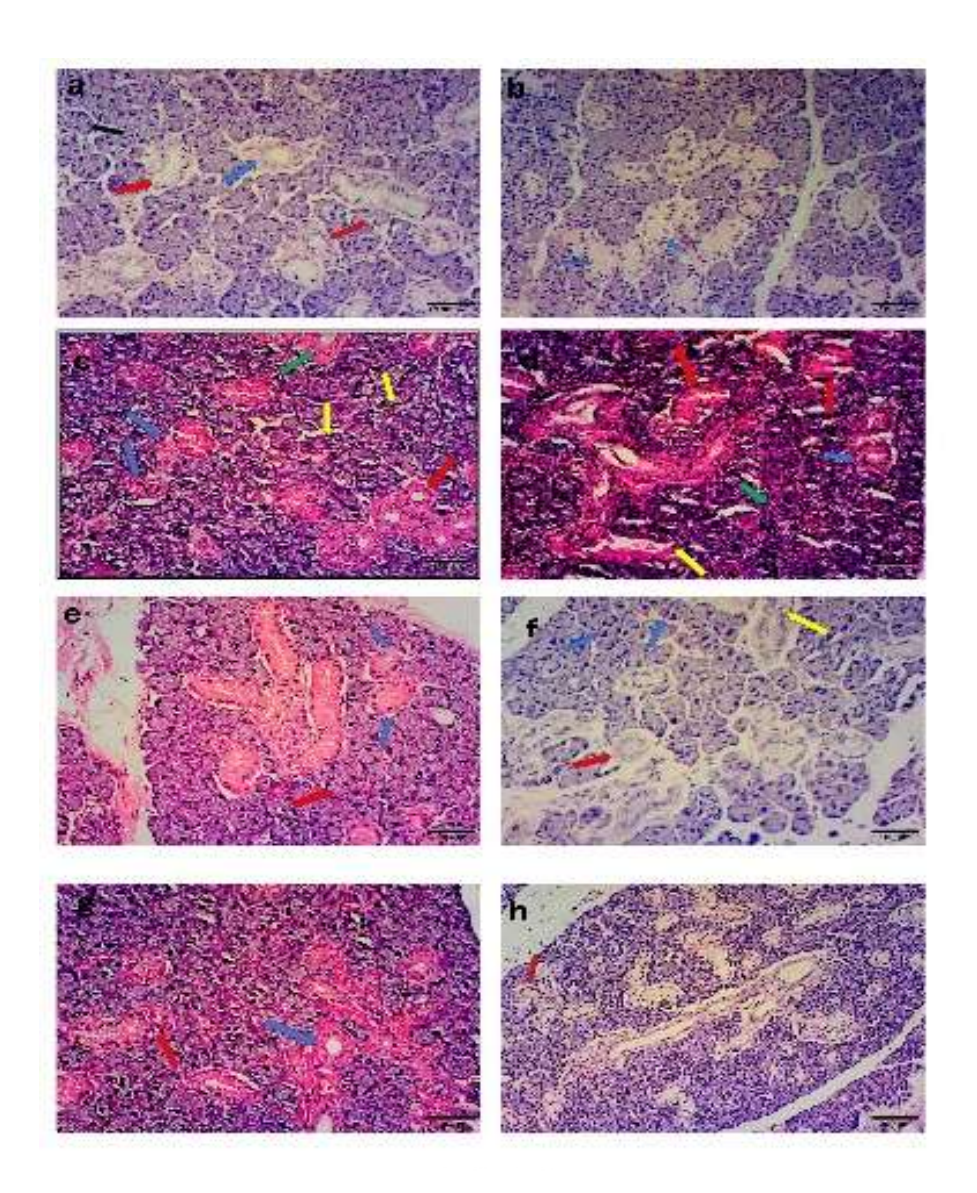


Fig. 1: A photomicrograph of: a: (IA) showing serous acini lined by pyramidal cells having basophilic cytoplasm and basally situated nuclei (Black arrow), normal appearance of SDs lined by columnar epithelium with centrally placed nucleus and eosinophilic basal striations (Blue arrow), and GCTs were lined by columnar cells with granular eosinophilic cytoplasm with basal rounded nuclei (Red arrow) (H&Ex200). b: (IB) showing normal appearance of GCTs with basal rounded nuclei and many eosinophilic granules (Blue arrows) (H&Ex200). c: (IIA) showing Multiple degenerated serous acini and abnormal nuclei (yellow arrow), SD with basal striations and patent lumen (red arrow) and other SDs with loss of basal striations and stagnated secretion (green arrow), GCT with ill-defined border (blue arrow) (H&Ex200). d: (IIB) showing multiple serous acini with hyperchromatic nuclei (green arrow), almost degenerated cells of SD with stagnation of secretion (yellow arrow) and SD showing loss of basal striations and hyperchromatic nuclei (blue arrow), GCT with partial loss of outline and hyperchromatic nuclei (red arrow)(H&Ex200).e:(IIIA) showing almost partial regeneration of serous acini (Red arrow), GCTs with normal outline and basal rounded hyperchromatic nuclei (Blue arrows)(H&Ex200). f:(IIIB) showing almost normal serous acini with multiple mitotic figures (Blue arrow), SDs with rounded nuclei and basal striations (Red arrow) and nearly normal granular element outline however some appear with cellular degeneration and cytoplasmic vacuoles(Yellow arrow)(H&Ex200).g: (IVA) showing almost normal SD (Blue arrow), GCTs have almost normal appearance with basal rounded nuclei and many eosinophilic granules however some show areas of cytoplasmic vacuoles (Red arrow)(H&Ex200).h: (IVB) showing almost normal outline of serous acini, SDs and GCTs. Note area of shrinkage (Red arrow) (H&Ex100).

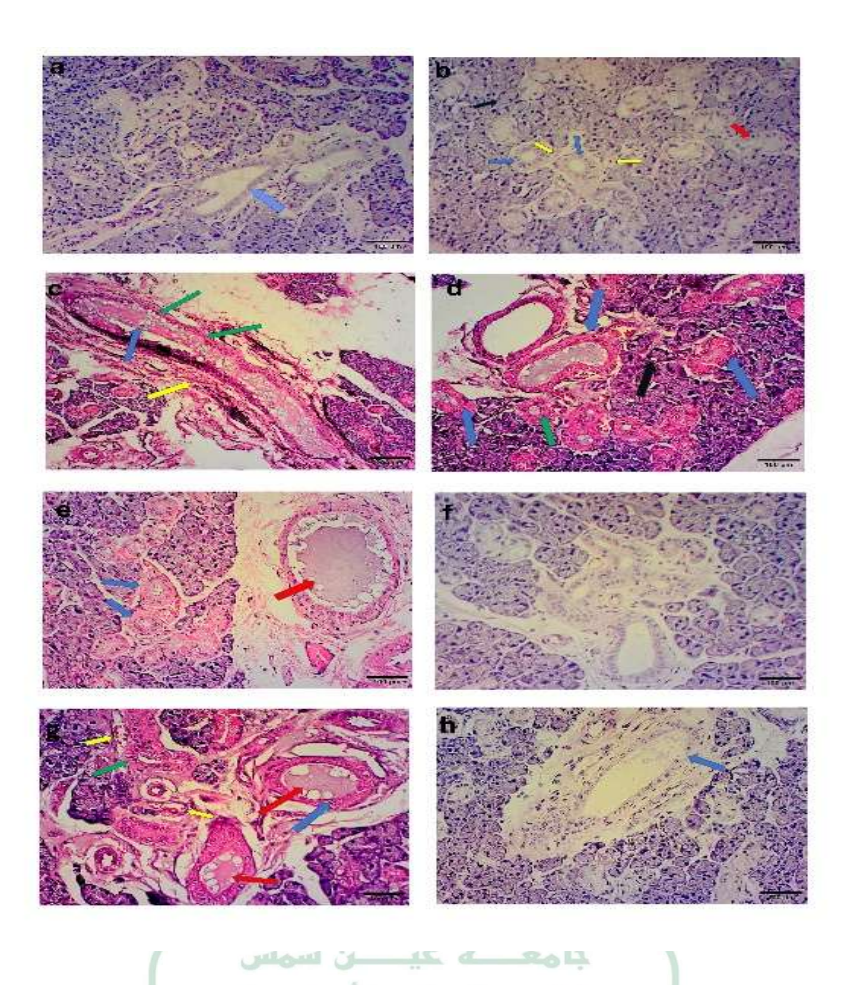


Fig. 2: A photomicrograph of: a: (IA) showing normal appearance of ED lined by pseudostratified columnar epithelium with goblet cells (Blue arrow) (H&Ex200), b: (IB) showing normal appearance of serous acini lined by pyramidal cells having basophilic cytoplasm and basally situated nuclei (Black arrow), SDs lined by columnar epithelium with centrally placed nucleus and eosinophilic basal striations (Blue arrow), Note associated BVs (Yellow arrow), and GCTs with basal rounded nuclei (Red arrow) (H&Ex200). c: (IIA) showing ED with stagnation of secretion (Blue arrow), degeneration of its lining cells with pyknotic nuclei and cytoplasmic vacuoles (green arrows) and surrounded by fibrosis (yellow arrow) (H&Ex100). d: (IIB) showing serous acini with cytoplasmic vacuolations and hyperchromatic nuclei (Black arrow), SDs with loss of basal striations and stagnated secretions (green arrow), Multiple EDs with stagnation of secretion (Blue arrows) (H&Ex200). e: (IIIA) showing almost normal SDs with basal striations (Blue arrows). Note ED with stagnated secretion (Red arrow) (H&Ex200). f: (IIIB) showing almost normal outline of serous acini, GCTs and ED(H&Ex200). g: (IVA) showing abnormal SDs with cytoplasmic vacuoles and stagnated secretion (Green arrow), ED lined by pseudostratified columnar epithelium with goblet cells with small areas of cytoplasmic vacuoles (Blue arrow) and stagnation of secretion in its lumen (Red arrow), Note associated congested BVs engorged with RBCs (Yellow arrow)(H&Ex200).h: (IVB) showing almost normal appearance of serous acini, ED lined by flat to cuboidal epithelium with areas of degeneration (Blue arrow), surrounded by nearly normal fibrous connective tissue (H&Ex200)

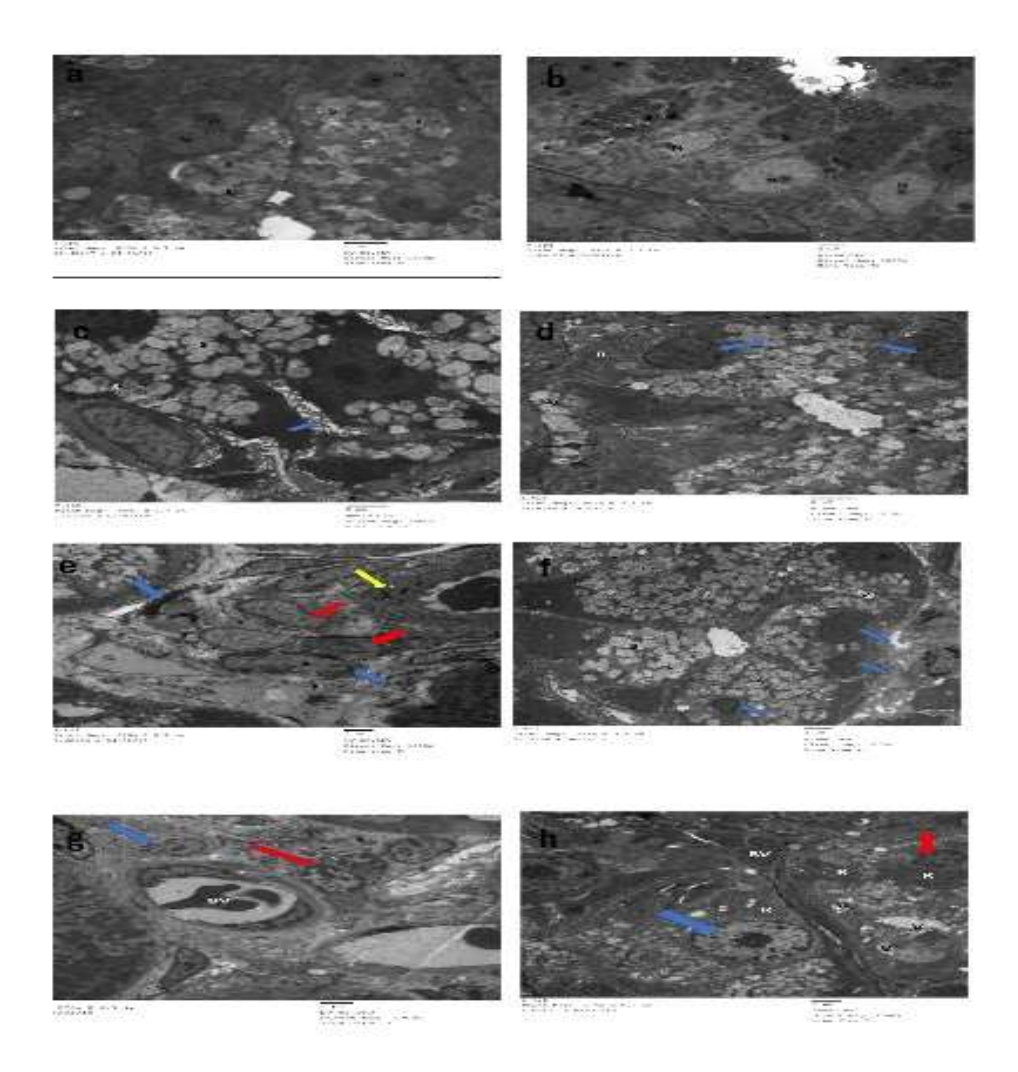


Fig. 3: An electron micrograph of: a: (IA) showing serous acinus with pyramidal cells, basal rounded nuclei (N), prominent nucleolus (n), and homogenous secretory granules (s). b: (IB) showing GCT with electron dense secretory granules (S), rounded nucleus (N) and prominent nucleolus(n). c: (IIA) showing detachment of cellular junctions between the atrophied acini (Blue arrow). Note multiple a typical secretory granule (S). d: (IIB) showing serous acinus with pyknotic nuclei (Blue arrows), dilated RER (R) and multiple cytoplasmic vacuoles (V). e: (IIIA) showing interstitial fibrosis (Blue arrows) and abnormal fibroblast with large plumb nucleus (Red arrows). Note blood vessel engorged with RBCs (BV) and surrounded by numerous collagen bundles (Yellow arrow). f: (IIIB) showing serous acinus with multiple secretory granules(S) and pleomorphic basal round nuclei (Blue arrows). Note cytoplasmic vacuoles(V). g: (IVA) showing macrophage (blue arrow) and lymphocyte (red arrow) infiltrated in connective tissue septa. Note blood vessel (BV) associated with endothelial cells and engorged with RBCs. h: (IVB) showing two adjacent acini in between blood vessels (BVs) associated with endothelial cell engorged with blood, open faced nucleus with prominent nucleolus (Blue arrow), pyknotic nucleus (Red arrow), cytoplasmic vacuoles (V) and dilated RER (R)((a,c,d)x1500, (b,e,f,g,h)x1000).

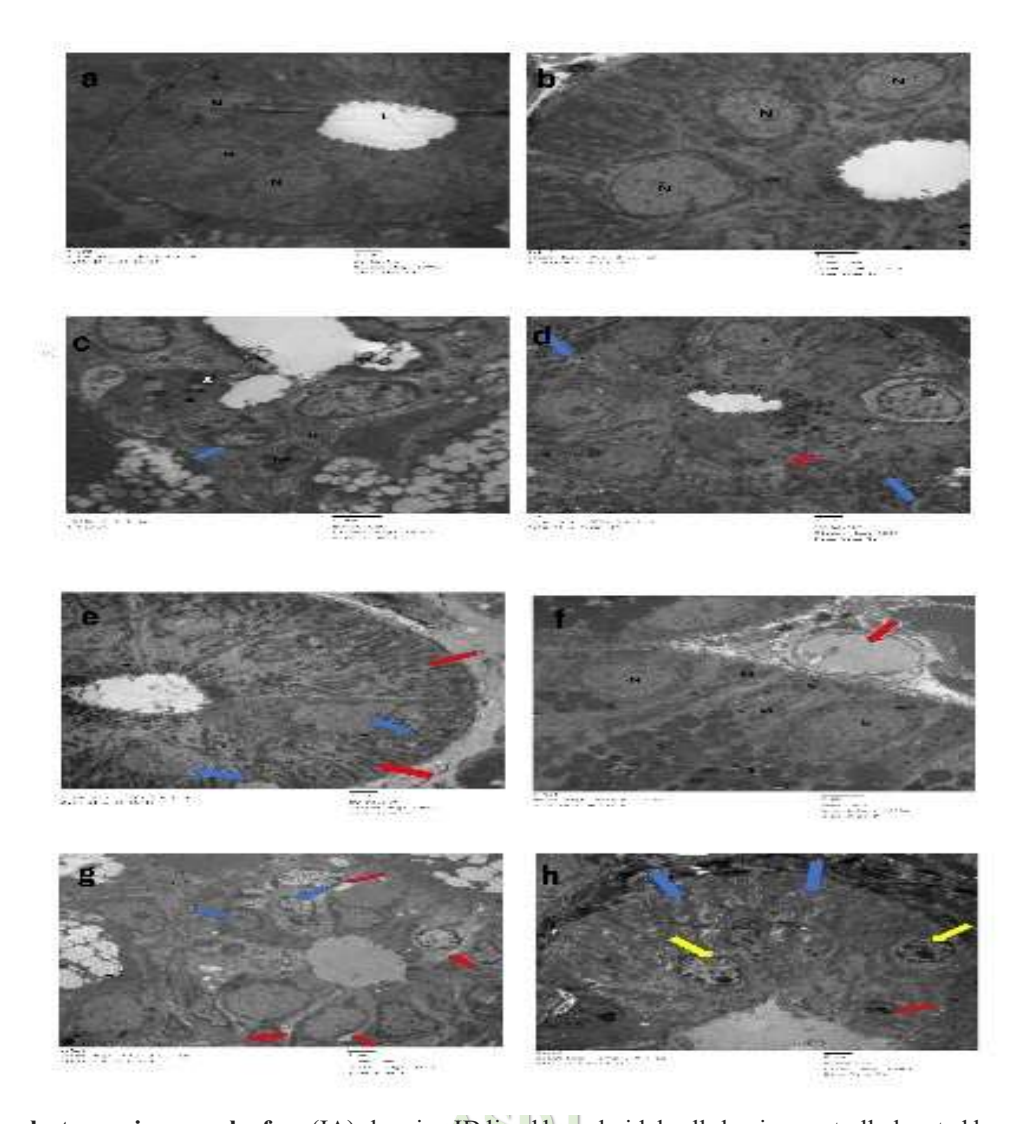


Fig. 4: An electron micrograph of: a: (IA) showing ID lined by cuboidal cells having centrally located large, rounded nuclei (N) and narrow lumen (L). b: (IB) showing SD having deep basal enfolding and open-faced nuclei with peripheral chromatin condensation (N). c: (IIA) showing ID with pyknotic nuclei (Blue arrow), secretory granules (S), dilated RER (R) and abnormal mitochondria (M). d: (IIB) showing SD with loss of basal striations (Blue arrows), abnormal pyknotic nucleus (Red arrow). e: (IIIA) showing SD with open faced nucleus (Blue arrows) and well-organized basal striations (Red arrows). f: (IIIB) showing GCT with numerous electron dense secretory granules(S), numerous mitochondria(M) and open-faced nucleus(N) with peripheral chromatin condensation. Note interstitial artery associated with endothelial cell (Red arrow). g: (IVA) showing ID with pleomorphic pyknotic nuclei and others with clumped chromatin (Blue arrows). Note multiple cytoplasmic vacuoles (Red arrows). h: (IVB) showing SD with normal basal striations (Blue arrows), open faced nucleus with prominent nucleolus but indented nuclear membrane (Yellow arrows) and pyknotic nucleus in different level (Red arrow) ((a,d,e,g,h)x1000, (b,c,f)x1500).

Quantitative real-time PCR results for genetic expression of TGFβ-1

All treated groups showed higher levels of TGF- $\beta 1$ than the irradiated group. After 7 days there was no statistically significant difference between IPRF group and exosomes group, with p-value (p>0.05). While after 14 days there was a statistically significant difference between them, with p-value (p<0.01), exosomes group being higher (Table. 1).

Table 1: showing mean \pm standard deviation (SD) of FC (TGF- β 1) gene expression for subgroup A and subgroup B

FC (TGF-β)	subgroup A	subgroup B	t-test	p-value
Group I	1.400±0.233	0.997±0.067	4.062	0.002*
Group 11	0.443±0.114	0.595±0.036	3.120	0.011*
Group III	0.731±0.118	4.410±0.745	11.941	0.001**
Group 1V	0.932±0.242	7.542±0.699	21.886	0.001**

SD: standard deviation, FC: fold change of tested gene after normalization to negative control.

^{*}p-value < 0.05 is significant

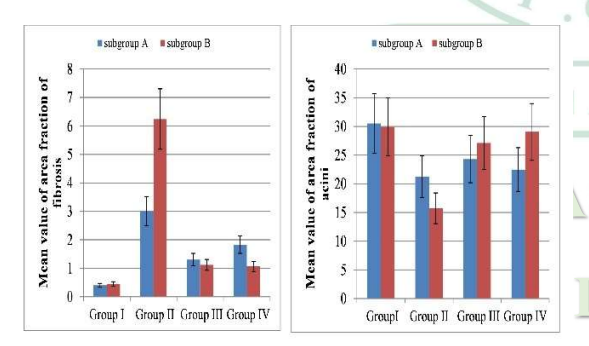


Fig 5: Comparison between subgroups A and B according to area fraction of fibrosis and acini in each group.

Discussion

H&E results of irradiated subgroups (IIA&IIB) in the present work revealed significant decrease in area fraction of the glandular acini (compared to other treated subgroups) and these finding were further emphasized by our electron microscopic results and are in accordance with Krishnan

et al.¹² This may be explained by acinus cell death, as for salivary glands, cell death consequent to radiation is attributed to multiple factors: apoptosis, necrosis, autophagy, senescence, activation of calcium channels in the cell membrane and depletion of stem/progenitor cells, all mediated by regulatory proteins, cytokines, chemokines and various signaling molecule.¹³

Regarding irradiated subgroups (IIA&IIB), increased intracytoplasmic vacuoles in acinar and ductal elements were markedly detected in both H&E and electron microscopic results. This could be attributed to the effect of irradiation on the acinar cell membrane causing its damage irregularities in the acinar cells downregulation of Aquaporin water channels (present at the apical membrane of acini) leading to decreased amylase secretion.¹² Cytoplasmic vacuolations may be also explained by production of Reactive oxygen species (ROS) that induce oxidative stress and cellular damage immediately following irradiation exposure. 14

Pyknotic nuclei, irregular nuclear membrane outline, hyperchromatic condensation and nuclear pleomorphism in irradiated subgroups (IIA&IIB) could be explained by DNA damage directly through double strand breakages or indirectly through reactive oxygen species (ROS) causing mutations and cell death.¹⁵ Mitochondrial disruption and damage could be attributed to accumulation of ca+ which mitochondrial ATPase activity and decreases energy generation. Damaged mitochondria and dilated RER would be a result of deficiency of protective enzymes, superoxide dismutase and glutathione peroxidase. ¹⁶

The SDs in irradiated group (IIA&IIB) exhibited loss of basal striations. This finding is due to the damage of mitochondria which was attributed to various lesions in the circular mitochondrial DNA. Stagnation of secretion in ED lumen could be

due to the pathological effect of radiotherapy on myoepithelial cells with failure of expelling the secretion into the oral cavity.¹⁸

Regarding fibrosis observed irradiated groups, Ionizing radiation can activate fibroblasts, endothelial cells and vascular smooth muscle cells, transforming them into myofibroblasts. These cells are involved in the secretion of extra cellular matrix.19 Another explanation is that radiation results in continuous ROS attack deregulation fibroblast of proliferation and metabolism and hence increases collagen expression.²⁰

TGF- β 1 gene expression in irradiated groups (IIA &IIB) revealed that there was a deficiency in this gene expression and these findings are in consistence with a previous study which demonstrated the effect of X-ray irradiation on the changes of expression of TGF- β in rat SMG. It was stated that TGF- β immunoreactivity decreased from day 10 post-irradiation and disappeared on day 30.²¹

TGF- β receptors are present in the basal and lateral membranes of acinar cells. Assembly of the intercellular junction of submandibular gland acinar cells may be affected by TGF- β induced by paracrine action of GCTs. ²² It was stated that there were alterations in expression of the tight junction genes claudin-3& claudin -4 occurred within 3 days of irradiation. So, Irradiation effect on cellular junctions may also affect TGF- β expression. ²³

The improved histological results in IPRF group (IIIA&IIIB) were consistent with a previous study which demonstrated that I-PRF increased SMGs' regenerative capacity by significantly reducing caspase-3 and by increasing vascular endothelial growth factors. ²⁴ Plumb fibroblast that appeared in subgroup IIIA may be due to biological activities of basic fibroblast growth factor present in IPRF including stimulation of fibroblast and capillary endothelial cells proliferation. Promotion of angiogenesis can

explain large BVs that were engorged with RBCs.²⁵

I-PRF is a fibrin network containing nanoscale fibers that scaffold cell proliferation, migration, and differentiation enhanced by its content of natural cocktail of growth factors which orchestrates tissue regeneration. This could explain the significant increase in acinar area fraction in IPRF group (IIIA&IIIB).²⁶

The apparent decrease in inflammatory **IPRF** signs in group (IIIA&IIIB) compared to the irradiated group (IIA&IIB) were represented by apparent decrease in extravasated RBCs, interstitial edema and shrinkage of acini which was further confirmed by significant increase in the acini area fraction. This result could be explained by PRF caused a robust inhibition of the inflammatory response to TNFα and IL1 β .²⁷

TGF-β1 gene expression showed statistically significant higher mean value in subgroup IIIB compared to subgroup IIIA, with p-value (p<0.01). It was stated that IPRF could induce higher cell migration and mRNA expression of TGF-β, PDGF, and type I collagen during tissue healing. TGF-β1 has been proved to stimulate extracellular matrix proteins formation by inducing the biosynthesis of collagen and laminin as well as promoting the expression of protease inhibitors, assessing regeneration of different tissues.

In the present work, exosomes subgroup IVB revealed superior histological results and significant increase in acini area fraction over both corresponding subgroups in both irradiated and IPRF group. This could be attributed to exosomes considered as active nanocomponents containing several regulatory factors, such as growth factors, cytokines, signaling lipids, messenger RNAs (mRNA), and non-coding RNAs (miRNAs), which play important roles in regulating other cellular processes in the surrounding

environment by MSCs.29 The RNA or proteins in MSC derived exosomes (MSC-Exos) can play a cell-homing role and regulate cell proliferation and differentiation, which can limit damage, regulate innate and adaptive immune responses, and promote self-repair and tissue regeneration after cell damage.30 Exosomes also have a role in reduction of ROS and oxidative stress. This could be attributed to their content of antioxidant molecules.31

The apparent decrease inflammatory signs in exosome group (subgroup IVA&IVB) compared to the irradiated group (subgroup IIA &IIB) was represented by an apparent decrease in interstitial edema and extravasated RBCs associated with significant increase in the acini area fraction. Exosomes transmit pro and anti-inflammatory miRNAs to neutralize an inflammatory reaction.³²

In the present study, there was a decrease in area fraction of fibrosis in exosome subgroups (IVA&IVB) compared to irradiated subgroups (IIA&IIB). It was demonstrated that in hepatic fibrosis models induced carbon tetrachloride, by transplantation of MSCs-derived exosomes epithelial could inhibit mesenchymal transition (EMT) in hepatocyte, alleviate inflammation, reduce collagen deposition, regulate fibrosis-related signaling pathways, thus improving liver fibrosis. It is suggested that MSC-derived exosomes might play a role in fibrotic diseases by reversing epithelial mesenchymal transition.³³

Exosomes subgroup (IVA &IVB) revealed a significant increase in TGFβ1 gene expression which used as regenerative marker compared with irradiated subgroups (IIA&IIB). These findings were consistent with a previous study which assessed regeneration of submandibular salivary glands bv measuring TGF_β1 immunohistochemically.³⁴

In the present work, area fraction of acini was higher in subgroup IIIA than subgroup IVA while area fraction of fibrosis of subgroup IIIA being lower. In a prior study that compared intraglandular injections of **PRF** and **ADSC** (adipose-derived mesenchymal stem cells) after 12 weeks of a single dose of irradiation, there was a nonsignificant difference in the ADSCs group compared to PRF group regarding cell proliferation using (PCNA). This finding supports our result regarding that PRF is a profound treatment but for a short-term duration.35

TGF-β1 gene expression was higher in subgroup IVA than subgroup IIIA, the difference being insignificant. It was suggested that I-PRF enhanced mRNA levels of TGF-β1 at 7 days.¹¹ However exosomes microRNAs regulate gene expression as many studies reported that microRNAs use exosomes as carrier to achieve cell to cell communication specifically exosomes microRNA which are secreted in the form of paracrine or remote secretion and taken by recipient cell targeting its mRNA 3'-UTR (mRNA regulator) results in down regulation of the Latent-transforming growth factor beta-binding protein 1(LTBP-1) which is one of inhibitory molecules of TGF-β1.³⁶ After 14 days exosomes subgroup IVB showed higher level of TGF-β1 gene expression. Accordingly, the interval time may play a role in SMG regeneration.³⁷

Conclusion

BM-MSCs derived exosomes and IPRF had a role in regeneration of irradiated SMG and increased expression of TGF-β1 gene. Our results demonstrated that using IPRF, an autologous treatment, had an ameliorative effect in regeneration irradiated SMG but for a short-term duration unlike exosomes that mediate a better regenerative effect on long term duration. investigations Further are needed

determine the possible ameliorative effect of both treatments when combined at different durations.

Funding source

This research did not receive any specific grant from funding agencies.

Data availability:

The datasets generated and / or analyzed during the current study are available from the corresponding author on reasonable request.

Ethical approval and consent to participate:

The experiment was conducted according to the "Guide for the Care and Use of Laboratory Animals" 8th ed., 2011, The Research Ethics Committee of the Faculty of Dentistry at Ain Shams University gave their approval for the experimental design (Approval number:FDASU-Rec IM 052331).

Competing interests

The authors assert explicitly that they have no known competing financial concerns or personal relationships with third parties that could appear to have influenced the effort disclosed in this study

References

- 1. Kordzińska-Cisek, I., & Grzybowska-Szatkowska, L. (2018). Salivary gland cancer epidemiology. Nowotwory. Journal of Oncology, 68(1), 22–27. https://doi.org/10.5603/NJO.2018.0005
- 2. Bray, F., Ferlay, J., Soerjomataram, I., Siegel, R. L., Torre, L. A., & Jemal, A. (2018). Global cancer statistics 2018: GLOBOCAN estimates of incidence and mortality worldwide for 36 cancers in 185 countries. CA: A Cancer Journal for Clinicians, 68(6), 394–424. https://doi.org/10.3322/CAAC.21492
- 3. Iozon, S., Caracostea, G. V., Páll, E., Şoriţău, O., Mănăloiu, I. D., Bulboacă, A. E., Lupşe, M., Mihu, C. M., & Roman, A. L. (2020). Injectable plateletrich fibrin influences the behavior of gingival mesenchymal stem cells. Romanian Journal of Morphology and Embryology, 61(1), 189–198. https://doi.org/10.47162/RJME.61.1.21
- 4. Zhang, J., Yin, C., Zhao, Q., Zhao, Z., Wang, J., Miron, R. J., & Zhang, Y. (2020). Anti-inflammation effects of injectable platelet-rich fibrin via

- macrophages and dendritic cells. Journal of Biomedical Materials Research Part A, 108(1), 61–68. https://doi.org/10.1002/JBM.A.36792
- 5. Shivashankar, V., Johns, D. A., Vidyanath, S., & Sam, G. (2013). Combination of platelet rich fibrin, hydroxyapatite and PRF membrane in the management of large inflammatory periapical lesion. Journal of Conservative Dentistry, 16(3), 261–264. https://doi.org/10.4103/0972-0707.111329
- 6. Lim, J. Y., Yi, T., Choi, J. S., Jang, Y. H., Lee, S., Kim, H. J., Song, S. U., & Kim, Y. M. (2013). Intraglandular transplantation of bone marrow-derived clonal mesenchymal stem cells for amelioration of post-irradiation salivary gland damage. Oral Oncology, 49(2), 136–143. https://doi.org/10.1016/J.ORALONCOLOGY.2012. 08.010
- 7. Fathy El-Tahawy, N. (2017). Effect of Platelet Rich Plasma (PRP) Injection on the Endocrine Pancreas of the Experimentally Induced Diabetes in Male Albino Rats: A Histological and Immunohistochemical Study. https://doi.org/10.4172/2155-6156.1000730
- 8. Du, Z., Wei, P., Jiang, N., Wu, L., Ding, C., & Yu, G. (2023). SHED-derived Exosomes Ameliorate Hyposalivation Caused by Sjögren Syndrome via Akt/GSK-3β/Slug-mediated ZO-1 Expression. Chinese Medical Journal. https://doi.org/https://doi.org/10.1097/cm9.0000000 000002610
- 9. Mohamed, N. H., Shawkat, S., Moussa, M. S., & Ahmed, N. E. B. (2022). Regeneration potential of bone marrow derived mesenchymal stem cells and platelet rich plasma (PRP) on irradiation-induced damage of submandibular salivary gland in albino rats. Tissue and Cell, 76, 101780. https://doi.org/10.1016/J.TICE.2022.101780
- 10. Zuo, R., Liu, M., Wang, Y., Li, J., Wang, W., Wu, J., Sun, C., Li, B., Wang, Z., Lan, W., Zhang, C., Shi, C., & Zhou, Y. (2019). BM-MSC-derived exosomes alleviate radiation-induced bone loss by restoring the function of recipient BM-MSCs and activating Wnt/β-catenin signaling. Stem Cell Research and Therapy, 10(1), 1–13. https://doi.org/10.1186/S13287-018-1121-9/FIGURES/7
- 11. Miron, R. J., Fujioka-Kobayashi, M., Hernandez, M., Kandalam, U., Zhang, Y., Ghanaati, S., & Choukroun, J. (2017). Injectable platelet rich fibrin (i-PRF): opportunities in regenerative dentistry? Clinical Oral Investigations, 21(8), 2619–2627. https://doi.org/10.1007/S00784-017-2063-9/FIGURES/5
- 12. Krishnan, M., Krishnan, M., Tennavan, A., Saraswathy, S., Sekhri, T., Singh, A. K., & Nair, V. (2017). Acute Radiation-Induced Changes in Sprague-Dawley Rat Submandibular Glands: A

- Histomorphometric Analysis. World Journal of Oncology, 8(2), 45–52. https://doi.org/10.4021/wjon.v8i2.1021
- 13. Acauan, M. D., Figueiredo, M. A. Z., Cherubini, K., Gomes, A. P. N., & Salum, F. G. (2015). Radiotherapy-induced salivary dysfunction: Structural changes, pathogenetic mechanisms and therapies. Archives of Oral Biology, 60(12), 1802–1810.
- $\label{eq:https://doi.org/10.1016/J.ARCHORALBIO.2015.09.014} https://doi.org/10.1016/J.ARCHORALBIO.2015.09.$
- 14. Srinivasan, M., Sudheer, A. R., Rajasekaran, K. N., & Menon, V. P. (2007). Effect of curcumin analog on γ-radiation-induced cellular changes in primary culture of isolated rat hepatocytes in vitro. Chemico-Biological Interactions, 176(1), 1–8. https://doi.org/10.1016/J.CBI.2008.03.006
- 15. Mahgoub, S., Sallam, A. O., Sarhan, H. K. A., Ammar, A. A. A., & Soror, S. H. (2020). Role of Diosmin in protection against the oxidative stress induced damage by gamma-radiation in Wistar albino rats. Regulatory Toxicology and Pharmacology, 113, 104622.
- https://doi.org/10.1016/J.YRTPH.2020.104622
- 16. El-Direny, E.A., Shalaby, N.M. and Afif, O.K. (2009) Effect of irradiation on secretory cells of submandibular gland of adult male albino rat. Histological and immunohistochemical study. Egyptian Journal of Histology, 32(2), 324-332.
- 17. Kam, W. W. Y., & Banati, R. B. (2013). Effects of ionizing radiation on mitochondria. Free Radical Biology and Medicine, 65, 607–619. https://doi.org/10.1016/J.FREERADBIOMED.2013. 07.024
- 18. Abd El-Haleem, M. R., Amer, M. G., Fares, A. E., & Kamel, A. H. M. (2022). Evaluation of the Radioprotective Effect of Silver Nanoparticles on Irradiated Submandibular Gland of Adult Albino Rats. A Histological and Sialochemical Study. BioNanoScience, 12(1), 13–27. https://doi.org/10.1007/S12668-021-00917-3/TABLES/2
- 19. Yu, W., Fu, J., Liu, Y., Wu, Y., & Jiang, D. (2018). Osteogenic protein-1 inhibits nucleus pulposus cell apoptosis through regulating the NF-κB/ROS pathway in an inflammation environment. Bioscience Reports, 38(6), 20181530. https://doi.org/10.1042/BSR20181530/98159
- 20. Zhang, T., Liu, C., Ma, S., Gao, Y., & Wang, R. (2020). Protective Effect and Mechanism of Action of Rosmarinic Acid on Radiation-Induced Parotid Gland Injury in Rats. Dose-Response, 18(1). https://doi.org/10.1177/1559325820907782/ASSET/IMAGES/LARGE/10.1177_1559325820907782-FIG4.JPEG

- 21. Choi, J. H., Wu, H.-G., Jung, K. C., Lee, S. H., & Kwon, E. K. (2009). Apoptosis and expression of AQP5 and TGF-beta in the irradiated rat submandibular gland. Cancer Research and Treatment, 41(3), 145. https://doi.org/10.4143/CRT.2009.41.3.145
- 22. Janebodin, K., Buranaphatthana, W., Ieronimakis, N., Hays, A. L., & Reyes, M. (2013). An In Vitro Culture System for Long-Term Expansion of Epithelial and Mesenchymal Salivary Gland Cells: Role of TGF-β1 in Salivary Gland Epithelial and Mesenchymal Differentiation. BioMed Research International, 2013(1), 815895. https://doi.org/10.1155/2013/815895
- 23. Yokoyama, M., Narita, T., Sakurai, H., Katsumata-Kato, O., Sugiya, H., & Fujita-Yoshigaki, J. (2017). Maintenance of claudin-3 expression and the barrier functions of intercellular junctions in parotid acinar cells via the inhibition of Src signaling. Archives of Oral Biology, 81, 141–150. https://doi.org/10.1016/J.ARCHORALBIO.2017.05.007
- 24. Elsherbini, A. M., & Ezzat, S. K. (2020). Effect of melatonin versus injectable platelet rich fibrin on critical wound healing in submandibular salivary glands of diabetic rats. Journal of Oral Biology and Craniofacial Research, 10(4), 592. https://doi.org/10.1016/J.JOBCR.2020.08.016
- 25. Amin, A.-R. E., Hosny, M. M., El-Destawy, M. T., & Abdel-Wahab, M. (2022). Comparison between PRP vs iPRF as an adjunct therapy in Infra-bony Pocket treatment. Al-Azhar Journal of Dental Science, 25(4), 485–493. https://doi.org/10.21608/AJDSM.2022.121791.1311 26. Varela, H. A., Souza, J. C. M., Nascimento, R. M., Araújo, R. F., Vasconcelos, R. C., Cavalcante, R. S., Guedes, P. M., & Araújo, A. A. (2019). Injectable platelet rich fibrin: cell content, morphological, and
- protein characterization. Clinical Oral Investigations, 23(3), 1309–1318. https://doi.org/10.1007/S00784-018-2555-2/FIGURES/8
 27. Kargarpour, Z., Nasirzade, J., Panahipour, L., Miron, R. J., & Gruber, R. (2021). Platelet-rich fibrin
- Miron, R. J., & Gruber, R. (2021). Platelet-rich fibrin decreases the inflammatory response of mesenchymal cells. International Journal of Molecular Sciences, 22(21), 11333. https://doi.org/10.3390/IJMS222111333/S1
- 28. Mansoub, N. H., Gürdal, M., Karadadas, E., Kabadayi, H., Vatansever, S., & Ercan, G. (2018). The role of PRP and adipose tissue-derived keratinocytes on burn wound healing in diabetic rats. BioImpacts: BI, 8(1), 5. https://doi.org/10.15171/BI.2018.02
- 29. Shafiaa, A. S. E., Baghdadi, H. M., Sabry, D., & Fouad, R. (2022). Effect of Mesenchymal Stem Cell-Derived Exosomes on Head & Neck Squamous Cell

Carcinoma Cell Line in Vitro Study. Ain Shams Dental Journal, 25(1), 74–83. https://doi.org/10.21608/ASDJ.2022.170792.1150 30. Di Trapani, M., Bassi, G., Midolo, M., Gatti, A., Kamga, P. T., Cassaro, A., Carusone, R., Adamo, A., & Krampera, M. (2016). Differential and transferable modulatory effects of mesenchymal stromal cell-derived extracellular vesicles on T, B and NK cell functions. Scientific Reports, 6. https://doi.org/10.1038/SREP24120

31. Salem, Z. A., Kamel, A. H. M., & AbuBakr, N. (2021). Salivary exosomes as a new therapy to ameliorate diabetes mellitus and combat xerostomia and submandibular salivary glands dysfunction in diabetic rats. Journal of Molecular Histology, 52(3), 467–477. https://doi.org/10.1007/S10735-020-09935-Z/FIGURES/7

32. Wu, J., Wang, Y., & Li, L. (2017). Functional significance of exosomes applied in sepsis: A novel approach to therapy. Biochimica et Biophysica Acta (BBA) - Molecular Basis of Disease, 1863(1), 292–297. https://doi.org/10.1016/J.BBADIS.2016.10.024
33. Li, T., Yan, Y., Wang, B., Qian, H., Zhang, X., Shen, L., Wang, M., Zhou, Y., Zhu, W., Li, W., & Xu, W. (2012). Exosomes Derived from Human Umbilical Cord Mesenchymal Stem Cells Alleviate Liver Fibrosis. Https://Home.Liebertpub.Com/Scd, 22(6), 845–854. https://doi.org/10.1089/SCD.2012.0395

34. Yasumitsu, T., Shimizu, O., Shiratsuchi, H., Miyake, Y., & Yonehara, Y. (2018). Distribution of aquaporin-5, transforming growth factor-β1 and laminin during regeneration of atrophic rat submandibular glands after duct ligation. Journal of Oral Science, 60(4), 595–600. https://doi.org/10.2334/JOSNUSD.17-0491

35. Wang, Z., Xing, H., Hu, H., Dai, T., Wang, Y., Li, Z., An, R., Xu, H., Liu, Y., & Liu, B. (2017). Intraglandular transplantation of adipose-derived stem cells combined with platelet-rich fibrin extract for the treatment of irradiation-induced salivary gland damage. Experimental and Therapeutic Medicine, 15(1), 795. https://doi.org/10.3892/ETM.2017.5497

36. Hu, X., Zhong, Y., Kong, Y., Chen, Y., Feng, J., & Zheng, J. (2019). Lineage-specific exosomes promote the odontogenic differentiation of human dental pulp stem cells (DPSCs) through TGFβ1/smads signaling pathway via transfer of microRNAs. Stem Cell Research and Therapy, 10(1), 1–14. https://doi.org/10.1186/S13287-019-1278-X/FIGURES/8

37. Janebodin, K., Buranaphatthana, W., Ieronimakis, N., Hays, A. L., & Reyes, M. (2013). An In Vitro Culture System for Long-Term Expansion of Epithelial and Mesenchymal Salivary Gland Cells: Role of TGF-β1 in Salivary Gland Epithelial and

Mesenchymal Differentiation. BioMed Research International, 2013. https://doi.org/10.1155/2013/815895

